WILEY | Hindawi

Research Article

Fabrication of C-Band High-Temperature Superconducting Microstrip Triplexer with High Accuracy

Runbo Jiang [iD],[1] **Wei Xie**,[2] **Shaoqi Yan**,[1] **Jinding Li**,[1] **Xiaoling Zhang**,[1] **Qingduan Meng** [iD],[1] **Jinhao Dai** [iD],[3] **Yuefeng Yuan** [iD],[3] **Chi Zhang**,[3] **Jia Wang** [iD],[3] **Chunguang Li** [iD],[3] **Yun Wu** [iD],[3] **Xu Wang** [iD],[3] **and Liang Sun** [iD][3]

[1]*Henan University of Science and Technology, Luoyang 471000, China*
[2]*Southwest China Research Institute of Electronic Equipment, Chengdu 610036, China*
[3]*Institute of Physics, Chinese Academy of Sciences, Beijing 100190, China*

Correspondence should be addressed to Qingduan Meng; qdmengly@163.com

This article presents a miniaturized C-band triplexer fabricated with high-temperature superconducting (HTS) microstrip lines and to be applied to quantum computers. The triplexer consists of three bandpass filters and branch lines. In the design of the bandpass filters, folded step impedance resonators (SIRs) are firstly used to achieve good stopband performances by harmonic suppression. Secondly, cross-coupling structures are also utilized to further improve the passband edge steepness of the bandpass filters. Finally, the parasitic transmission zeros originating from the assembling box sizes are employed to achieve a deeper out-of-band rejection. Three bandpass filters are designed and connected to the common input port of the triplexer. After that, the triplexer is coarsely optimized by advanced design system (ADS) for time-saving and is finely optimized by Sonnet for better accuracy. The optimized layout of the triplexer is fabricated on a 2-inch diameter and 0.5 mm thickness MgO wafer; here, the MgO wafer is double-sided coated with HTS $YBa_2Cu_3O_7$ (YBCO) thin films. The measured passband bandwidths (return loss greater than 12 dB) of the triplexer are 6.420-6.680 GHz, 6.780-7.030 GHz, and 7.110-7.380 GHz, respectively, which satisfy the required design specifications.

1. Introduction

At frequencies below 10 GHz, the surface resistivity of HTS is less than 5×10^{-4} ohm. This unique feature makes HTS microstrip filters with lower insertion loss and deeper out-of-band rejection [1]. Multiplexers are widely used in satellite communications, radars, and electronic warfare, and they split the input wideband signals into several narrowband signals, and vice versa. Multiplexers are implemented by using the circulator, the hybrid-coupled structure, the common-coupled resonator structure, and the manifold-coupled structure [2–7]. The manifold-coupled structure is extensively adopted in multiband communication systems owning to its compactness. Some optimization methods were also adopted in the design of multiplexers [8–12]. In

this paper, we present the development of a miniaturized C-band microstrip HTS triplexer employed in quantum computers, where noise and interference added to the microwave signals controlling the quantum bits can be filtered out by microstrip HTS triplexers with high performance [13, 14]. The compact triplexer is designed with a branch structure and three bandpass filters. As the number of the channel filters increases, more time is needed to optimize the branch structure because of the increasing constraints among channels. To tackle this problem, ADS is firstly employed to achieve coarse adjustment of the triplexer, and Sonnet is then employed to achieve fine adjustment of the triplexer for better accuracy. All these approaches guarantee that the measured responses of the fabricated triplexer satisfy the required index.

2. Triplexer Design

The required frequency ranges for the three channels of the triplexer are 6.400-6.700 GHz (channel A), 6.750-7.050 GHz (channel B), and 7.100-7.400 GHz (channel C), respectively. The guard band between the three channels is 50 MHz. To achieve a deeper out-of-band rejection and the compactness of the channel filters, a six-order quasielliptic function filter with a pair of transmission zeros is chosen for each channel filter. According to the coupling matrix synthesis methods [15], the coupling coefficients and the external quality factors were obtained and listed in Table 1. Here, the coupling coefficients are identical because each channel filter has the same bandwidth.

2.1. Bandpass Filter Design. The three channel filters are designed and simulated with Sonnet. Step impedance resonators (SIRs) are selected to build the bandpass filters to achieve a wider out-of-band rejection and are folded for compactness, as shown in Figure 1. The widths of the open stubs and the high impedance lines in the SIR are 0.27 mm and 0.06 mm, respectively. The gap between the open stubs of the SIR is 0.09 mm. Compared with traditional resonators, the wider open stubs of the SIR increase the loading capacitance to ground. This enlarged capacitor increases the ratio of the second resonant frequency to the fundamental resonant frequency. Besides, the wider open stubs of the SIR also increase the planar capacitance consisting of the open stubs and the gap between them. This increased planar capacitor is beneficial for reducing the dimensions of the resonators. This folded SIR structure is flexible to realize the electric coupling and the magnetic coupling by simply flipping the adjacent resonators because of its nonsymmetry structure. The final layout of the SIR is $0.02 \lambda_g \times 0.04 \lambda_g$. Here, λ_g represents the guided wavelength at the center frequency of the channel A.

The coupling coefficients are calculated from Equation (1), where f_1 and f_2 represent the resonant frequencies between two neighboring coupled SIR resonators, and the effect from two terminals should be weak enough. The external quality factor is calculated from Equation (2), where ω_0 is the resonant frequency of the SIR; $\Delta \omega_{\pm 90°}$ are determined from the frequency at which the phase shifts $\pm 90°$ with respect to the absolute phase at ω_0. The coupling matrix is calculated from Equation (3), where FBW is the fractional bandwidth. [16].

$$M_{i,j} = \pm \frac{f_2^2 - f_1^2}{f_2^2 + f_1^2}, \tag{1}$$

$$Q_e = \frac{\omega_0}{\Delta \omega_{\pm 90°}}, \tag{2}$$

$$m_{i,j} = \frac{M_{i,j}}{\text{FBW}}. \tag{3}$$

With the folded SIR resonator and the synthesized coupling matrices, the layout of each channel filter can

TABLE 1: Coupling coefficients and external quality factors of the channel filters.

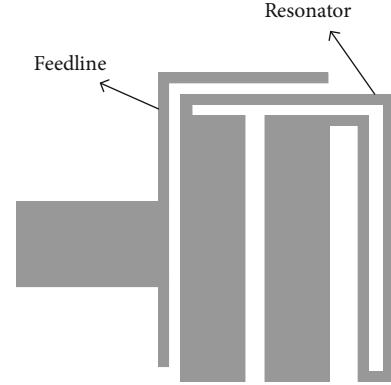| Channel	$m_{12} = m_{56}$	$m_{23} = m_{45}$	m_{34}	m_{25}	Q_e
Channel A	0.827	0.566	0.728	-0.187	22.10
Channel B	0.827	0.566	0.728	-0.187	23.28
Channel C	0.827	0.566	0.728	-0.187	24.47

FIGURE 1: Folded stepped impedance resonator and feedline structure.

be obtained by Sonnet. Figure 2 is the layout of the channel A, its size is $0.15 \lambda_g \times 0.05 \lambda_g$. The width of the feed lines is set to be 0.5 mm. The gaps between the resonators are $g_1 = 0.12$ mm, $g_2 = 0.35$ mm and $g_3 = 0.22$ mm, respectively. The simulated response curves of the channel A are plotted with black lines and shown in Figure 3. Apparently two pairs of transmission zeros appear and locate on both sides of the passband. One pair of transmission zeros ($TZ_1 = 6.360$ GHz and $TZ_2 = 6.750$ GHz) originate from the cross-coupling between the line connecting the second and the fifth resonators. The other pair of transmission zeros ($TZ_3 = 6.210$ GHz and $TZ_4 = 7.120$ GHz) are mainly determined by the width of the assembly box and move away from the passband when the width of the assembly box decreases from 9 mm to 6 mm in steps of 1.5 mm. The corresponding out-of-band rejection level is improved from -55 dB up to -65 dB. The dependence of the transmission zeros on the box sizes is shown in Figures 4(a) and 4(b). Both the width and the length of the box affect the 2nd pair of transmission zeros, and hardly influence the 1st pair of transmission zeros. The layouts of the channel B and the channel C are also obtained by repeating the design process described above.

2.2. Branch Lines Design and Optimization. When the design of the three bandpass filters is completed, the branch lines are connected to the three bandpass filters. Non-optimized branch lines greatly worsen the transmission responses of the channel filters due to impedance mismatch. So, reducing impedance mismatch is essential and is achieved by adjusting the lengths of the branch lines [17]. Usually, the lengths of branch lines need
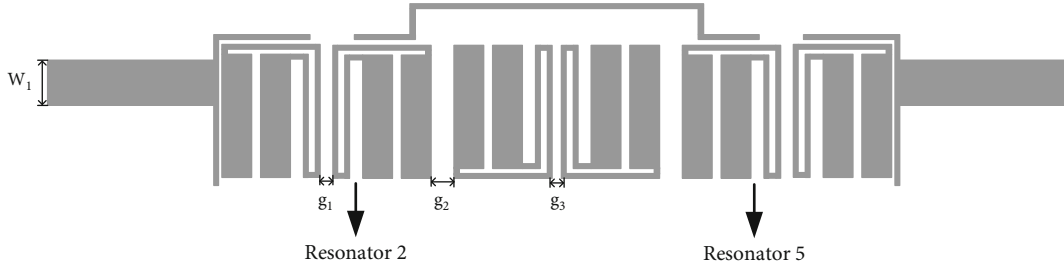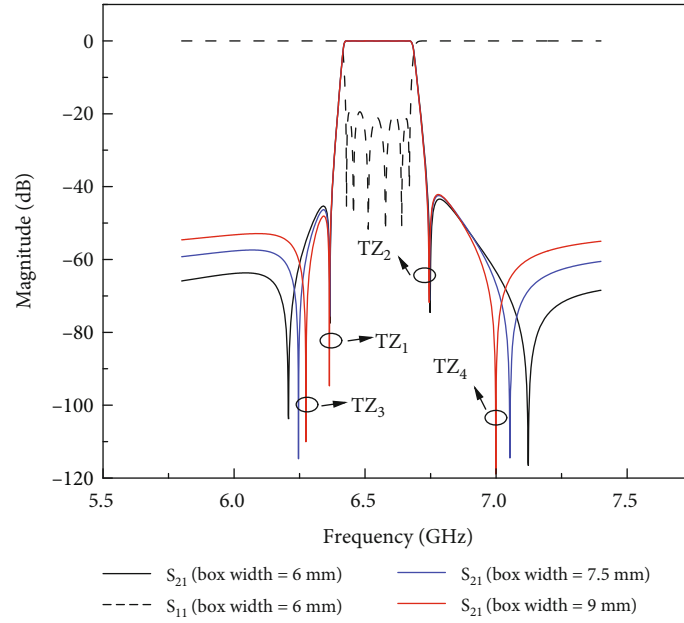
FIGURE 2: Layout of the channel A.

FIGURE 3: Comparison of the simulated S_{21} of the channel A filter with different box widths.

to satisfy the following constraints:

$$Z_{inA}(f_A) = 50\,\Omega, \quad Z_{inB}(f_A) = Z_{inC}(f_A) = \infty, \qquad (4)$$

$$Z_{inB}(f_B) = 50\,\Omega, \quad Z_{inA}(f_B) = Z_{inC}(f_B) = \infty, \qquad (5)$$

$$Z_{inC}(f_C) = 50\,\Omega, \quad Z_{inA}(f_C) = Z_{inB}(f_C) = \infty, \qquad (6)$$

$$2n\frac{\lambda_j}{4} - 0.3\lambda_j < L_{ij} < 2n\frac{\lambda_j}{4} + 0.3\lambda_j \; n = 1, 2, 3 \cdots, \qquad (7)$$

where Z_{ink}, $k = A$, B, or C, is the input impedance defined at the input port of branch lines shown in Figure 5. f_A, f_B, and f_C represent the center frequencies of the channels A, B and C, respectively. Specifically, the lengths of the branch lines can be calculated from Equation (7), where λ_j is the wavelength in the channel j ($j = A$, B and C), and L_{ij} ($i = A$, B and C) are the branch lengths connecting any two input feed lines of the three channel filters [18].

After calculating the initial values of L_{ij}, the layout of the triplexer should be optimized by a full-wave electromagnetic (EM) simulator. However, the optimization of

the branch lines is very time-consuming. For time saving, the circuit-theory model is firstly used to obtain initial parameters of the branch lines, and an EM simulator is employed to find the optimal parameters of the branch lines. The branch lines are built by microstrip line, microstrip open stub, microstrip T-junction, and microstrip corner component in ADS. The S-parameters of the channels A, B and C obtained in Sonnet are imported into ADS. The lengths of the branch lines are set as variable, and their initial lengths are calculated by Equations (4)–(7). Moreover, the layout of the branch lines should be compact and can be loaded onto a two-inch MgO substrate. For easy calculation, we employ L_1, L_2, L_3, L_4, L_5, L_6 replacing the former mentioned L_{ij} as variable parameters. After optimization in ADS, the optimal lengths are listed as $L_1 = 3.36$ mm, $L_2 = 6.00$ mm, $L_3 = 2.18$ mm, $L_4 = 1.55$ mm, $L_5 = 4.66$ mm, and $L_6 = 1.41$ mm.

2.3. Optimization of Triplexer. Microstrip lines are described with empirical models in ADS, and the mutual influence between the branch lines and the filters is also ignored. The added branch lines have a great influence on the coupling parameters of the resonators connected with the
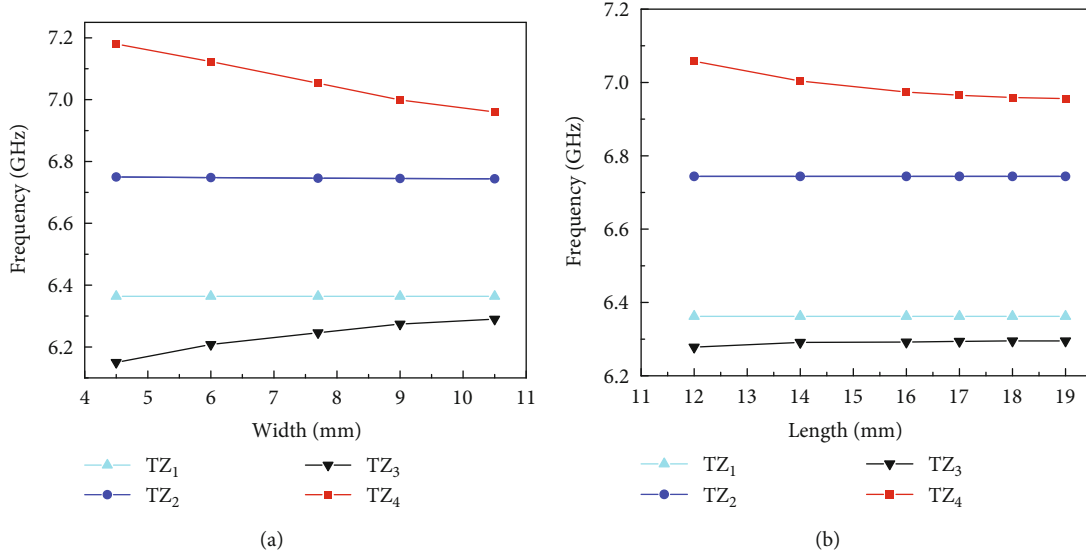
FIGURE 4: (a) Transmission zeros dependence of the box widths. (b) Transmission zeros dependence of the box lengths.
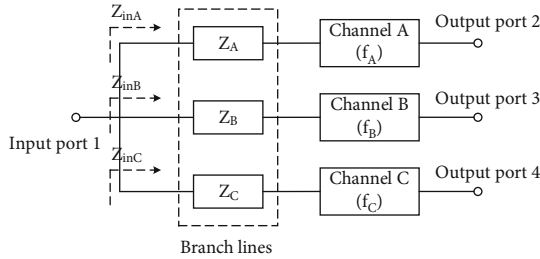

FIGURE 5: Block diagram of the triplexer.

FIGURE 6: Final layout of the triplexer.

manifold. Therefore, the triplexer needs to be optimized by EM simulator. The optimized layout is shown in Figure 6. The optimal lengths of the branch lines are listed as $L_1 = 4.86$ mm, $L_2 = 5.17$ mm, $L_3 = 2.93$ mm, $L_4 = 2.53$ mm, $L_5 = 4.71$ mm, and $L_6 = 2.33$ mm. For easy assembly, four SMA connectors connected with port 1, port 2, port 3, and port 4 are folded and placed at the center of four sides of the assembly box, as shown in Figure 7. The size of the triplexer is $0.40 \lambda_g \times 0.40 \lambda_g$.

Simulated responses of the designed triplexer are shown in Figures 8(a), 8(b), and 9. Its 3 dB passband ranges are 6.402-6.690 GHz, 6.750-7.043 GHz, and 7.102-7.395 GHz, respectively, and the return losses are better than 20 dB in all channels. The isolation between the three passbands is better than 35 dB, as shown in Figure 10.

3. Fabrication and Measurements

When the optimization of the triplexer is completed, its microstrip layout is transferred onto a mask with the minimum gap of 0.02 mm between the adjacent lines. After photolithography and ion-beam etching, the microstrip circuit of the triplexer is presented on a 2-inch and 0.50-mm thick MgO substrate coated with YBCO films. Then, the MgO wafer is diced and assembled in a gold-plated box. The size
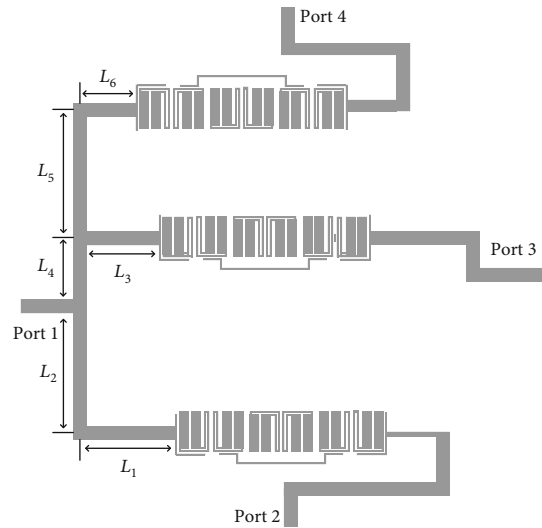
of the assembled triplexer, including four SMA ports, is 51 mm × 51 mm × 15 mm, and the photograph of the assembled triplexer is shown in Figure 7.

The triplexer is mounted in a cryogenic cooler at room temperature, cooled down to 45 K, and measured with a network analyzer shown in Figure 11. Calibration is performed before measurement. The measured results are shown in Figures 8 and 9. The measured results agree very well with the simulated results. To be more specific, the measured 3 dB passbands of the triplexer are 6.398-6.679 GHz, 6.748-7.033 GHz, and 7.096-7.385 GHz, respectively. The passband bandwidths (return loss better than 12 dB) of the triplexer are 6.420-6.680 GHz, 6.780-7.030 GHz, and 7.110-7.380 GHz, respectively. The insertion losses at the center frequencies of the three channels are 0.25 dB, 0.20 dB, and 0.13 dB, respectively. We consider that the gold wires bonded with the SMAs may be mainly the source of the
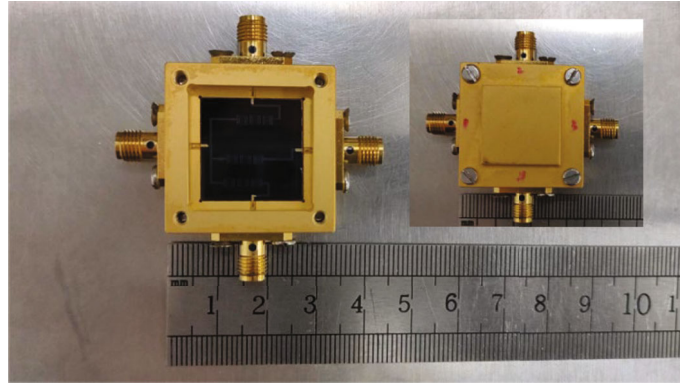
FIGURE 7: Photograph of the assembled triplexer.
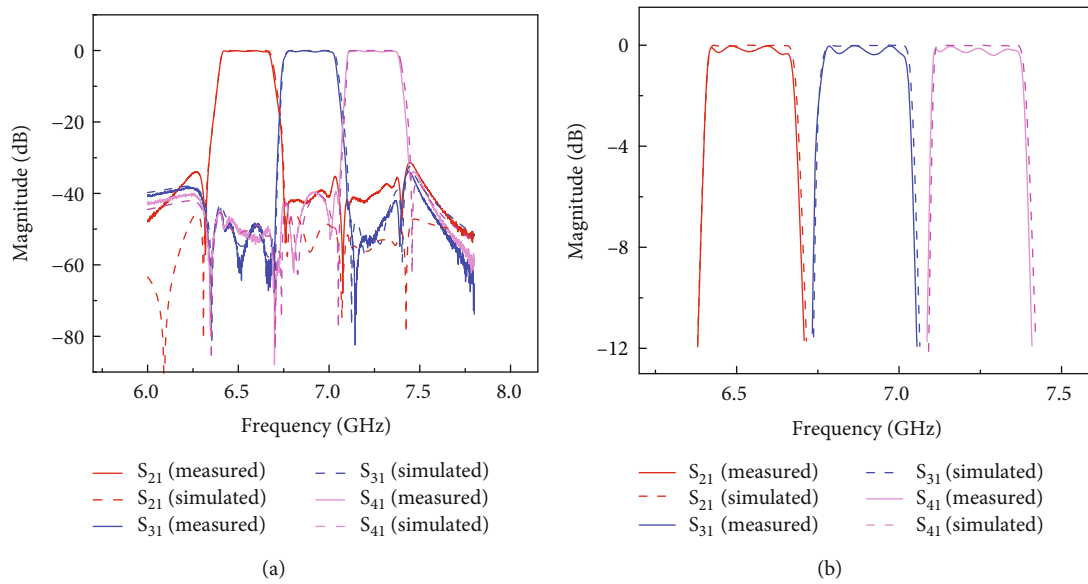

(a)

(b)

FIGURE 8: (a) EM simulation and measurement results of the triplexer. (b) Amplifying passband response of the triplexer.
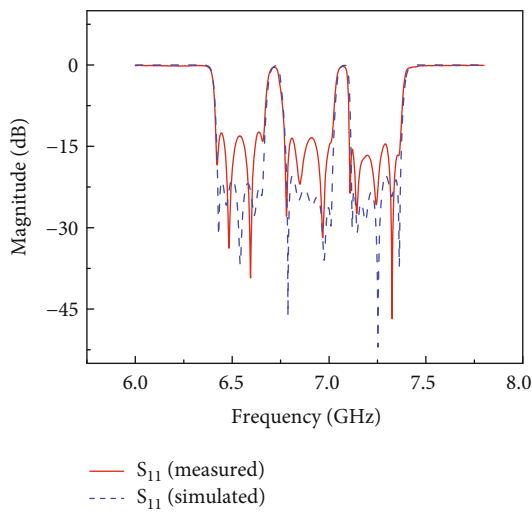

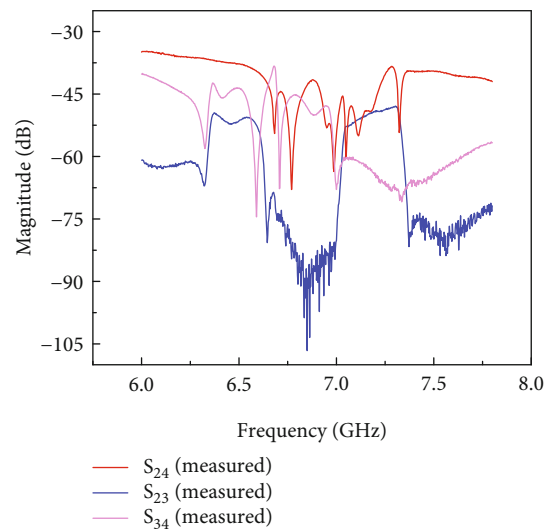FIGURE 9: Measured and simulation reflection loss of the triplexer.

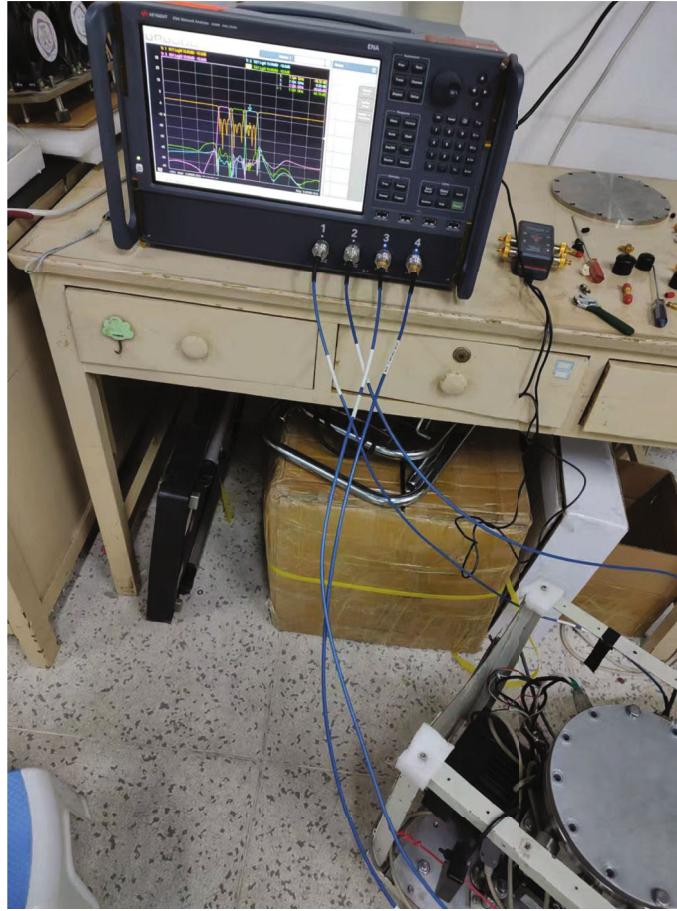FIGURE 10: Measured isolation responses of the triplexer.

Figure 11: Photograph of the measurement setup.

Table 2: Simulated and measured frequency response of the triplexer.

Specifications	Channel A (GHz)	Channel B (GHz)	Channel C (GHz)
Required passband range	6.400-6.700	6.750-7.050	7.100-7.400
Simulated passband range	6.402-6.690	6.750-7.043	7.102-7.395
Measured passband range (3 dB)	6.398-6.679	6.748-7.033	7.096-7.385
Measured passband (return loss better than 12 dB)	6.420-6.678	6.780-7.030	7.110-7.380
Simulated bandwidth shrinkage ratio	-4.0%	-2.3%	-2.3%
Measured bandwidth shrinkage (3 dB) ratio	-6.3%	-5.0%	-3.7%
Measured bandwidth ratio (return loss better than 12 dB)	-14.0%	-16.7%	-10.0%

insertion losses. The isolation among the three channels is better than 35 dB as shown in Figure 10. Details of the simulated and measured specifications of the triplexer are listed in Table 2.

We observe that the start frequencies of the triplexer are closer to the required start frequencies, but the cut-off frequencies are slightly deviated from the required cut-off frequencies. The measured bandwidth shrinkage ratio is not larger than 6.5%. The measured return losses of the three channels decreased down to 12 dB from the simulated 20 dB due to the inevitable fabrication errors, which may originate from the dielectric constant inhomogeneity of MgO substrate and ion-beam etching.

4. Conclusions

A compact C-band microstrip HTS triplexer has been presented in this article. The triplexer is composed of three bandpass filters and branch lines. Both the cross-coupling between resonators and the added coupling path originated from the assembled box are employed to generate two pairs of transmission zeros to improve the edge steepness of a bandpass filter. A time-saving optimization step is proposed to optimize the branch lines. The measured results are in good agreement with the simulated results and meet the requirement of the project.

Data Availability

Conflicts of Interest

There is no conflict of interest regarding the publication of this paper.

Acknowledgments

References

[1] C. Zhang, W. Xie, C. Li et al., "Recent progress on high-temperature superconducting filters," *Superconductivity*, vol. 2, article 100012, 2022.

[2] E. Belohoubek, E. Denlinger, D. Kalokitis et al., "Advanced high-temperature superconducting components for microwave systems," *Journal of Superconductivity*, vol. 5, no. 4, pp. 423–429, 1992.

[3] S. Hong and K. Chang, "A 10-35-GHz six-channel microstrip multiplexer for wide-band communication systems," *IEEE Transactions on Microwave Theory and Techniques*, vol. 54, no. 4, pp. 1370–1378, 2006.

[4] R. R. Mansour, S. Ye, V. Dokas et al., "Design considerations of superconductive input multiplexers for satellite applications," *IEEE Transactions on Microwave Theory and Techniques*, vol. 44, no. 7, pp. 1213–1228, 1996.

[5] C.-F. Chen, T.-Y. Huang, C.-P. Chou, and R.-B. Wu, "Microstrip diplexers design with common resonator sections for compact size, but high isolation," *IEEE Transactions on Microwave Theory and Techniques*, vol. 54, no. 5, pp. 1945–1952, 2006.

[6] M. M. Mendoza, M. G. Tudela, and R. G. C. Camuñas, "Design of a four channel C-band multiplexer with a modified star-junction topology," in *2020 IEEE/MTT-S International Microwave Symposium (IMS)*, pp. 587–590, Los Angeles, CA, USA, 2020.

[7] G. Macchiarella and S. Tamiazzo, "Synthesis of star-junction multiplexers," *IEEE Transactions on Microwave Theory and Techniques*, vol. 58, no. 12, pp. 3732–3741, 2010.

[8] J. C. Melgarejo, J. Ossorio, S. Cogollos, M. Guglielmi, V. E. Boria, and J. W. Bandler, "On space mapping techniques for microwave filter tuning," *IEEE Transactions on Microwave Theory and Techniques*, vol. 67, no. 12, pp. 4860–4870, 2019.

[9] M. A. Ismail and M. Yu, "Advanced design of large-scale microwave devices for space applications using space mapping optimization," in *2017 IEEE MTT-S International Microwave Symposium (IMS)*, pp. 1515-1516, Honololu, HI, USA, 2017.

[10] Z. Zhang, H. Chen, Y. Yu, F. Jiang, and Q. S. Cheng, "Yield-constrained optimization design using polynomial chaos for microwave filters," *IEEE Access*, vol. 9, pp. 22408–22416, 2021.

[11] C. Hu and B. D. Youn, "Adaptive-sparse polynomial chaos expansion for reliability analysis and design of complex engineering systems," *Structural and Multidisciplinary Optimization*, vol. 43, no. 3, pp. 419–442, 2011.

[12] E. H. Sandoval, F. Anstett-Collin, and M. Basset, "Sensitivity study of dynamic systems using polynomial chaos," *Reliability Engineering & System Safety*, vol. 104, pp. 15–26, 2012.

[13] D. Ristè, S. Poletto, M.-Z. Huang et al., "Detecting bit-flip errors in a logical qubit using stabilizer measurements," *Nature Communications*, vol. 6, no. 1, p. 6983, 2015.

[14] Y. He, J. Liu, C. Zhao, R. Huang, G. Dai, and W. Chen, "Control system of superconducting quantum computers," *Journal of Superconductivity and Novel Magnetism*, vol. 35, no. 1, pp. 11–31, 2022.

[15] R. J. Cameron, "General coupling matrix synthesis methods for Chebyshev filtering functions," *IEEE Transactions on Microwave Theory and Techniques*, vol. 47, no. 4, pp. 433–442, 1999.

[16] J. S. Hong and M. J. Lancaster, *Microstrip Filters for RF/Microwave Applications*, John Wiley & Sons, 2004.

[17] P. D. Laforge, R. R. Mansour, and M. Yu, "Reconfigurable MEMS-based BPF for manifold-coupled-superconducting triplexers," *IEEE Transactions on Applied Superconductivity*, vol. 28, no. 6, pp. 1–8, 2018.

[18] P. H. Deng, M. I. Lai, S. K. Jeng, and C. H. Chen, "Design of matching circuits for microstrip triplexers based on stepped-impedance resonators," *IEEE Transactions on Microwave Theory and Techniques*, vol. 54, no. 12, pp. 4185–4192, 2006.